Vibrational properties of water molecules adsorbed in different zeolitic frameworks

2006 J. Phys.: Condens. Matter 18 3563

(http://iopscience.iop.org/0953-8984/18/15/004)

INSTITUTE OF PHYSICS PUBLISHING JOURNAL OF PHYSICS: CONDENSED MATTER

J. Phys.: Condens. Matter **18** (2006) 3563–3580 doi:10.1088/0953-8984/18/15/004

Vibrational properties of water molecules adsorbed in different zeolitic frameworks

V Crupi, F Longo, D Majolino and V Venuti

Department of Physics, University of Messina, Contrada Papardo, Salita Sperone 31, PO Box 55, 98166 S Agata, Messina, Italy

E-mail: vvenuti@unime.it

Received 8 July 2005, in final form 20 January 2006
Published 30 March 2006
Online at stacks.iop.org/JPhysCM/18/3563

Abstract

The perturbation of water 'sorbed' in samples of zeolites of different structural type, genesis, and cation composition (K-, Na-, Mg- and Ca-rich zeolites), namely the CHA framework of a synthetic K-chabazite, the LTA framework of synthetic Na-A and Mg50-A zeolites, and the NAT framework of a natural scolecite, has been studied by FTIR-ATR spectroscopy, in the −10 to +80 °C temperature range. The aim was to show how differences in the chemical composition and/or in the topology of the zeolite framework and, in particular, the possibility for the guest water molecules to develop guest–guest and/or host–guest interactions, lead to substantial differences in their vibrational dynamical properties.

The spectra, collected in the O–H stretching and H_2O bending mode regions, are complex, with multiple bands being observed.

As far as water in the CHA and LTA frameworks is concerned, whose behaviour is governed by the balance of water–water, water–framework and water–extra-framework cations interactions, the assignment of the resolved components of the O–H stretching band has been discussed by fitting the band shapes into individual components attributed to H_2O molecules engaged in different degrees of hydrogen bonding. A detailed quantitative picture of the connectivity pattern of water, as a function of temperature and according to the chemical and topological properties of the environment, is furnished. The H_2O bending vibrational bands give additional information that perfectly agrees with the results obtained from the analysis of the O–H stretching spectral region.

In the case of scolecite, a small-pored zeolite where water–water interactions are eliminated, the increased complexity observed in the infrared spectra in the O–H stretching and H_2O bending regions was explained as due to the hydrogen bonding between the water molecules and the network, and also with the extra-framework cation. Furthermore, these observations have been correlated with the different O···O bond distances of the water molecules in the NAT framework.

1. Introduction

Nanoscopic confinement has recently attracted increasing interest from the point of the basic research, in studying the influence of finite size effects on the structure and dynamics of a liquid, and in view of the numerous technological applications [1–6]. In particular, as shown by the conspicuous literature in this field, the knowledge of the dynamics of confined water and its relation with the bulk state is at the basis of the comprehension of a lot of technological, geological and biological problems [7–20]. Water at a protein surface, such an example, has been shown to be relevant to protein stability and function [21]. These studies are also of relevance for a better understanding of the phase diagram of water. In fact, a supercooled, non-freezing behaviour has been evidenced for water confined between layers of phospholipids, trapped in amorphous porous materials and phyllosilicates [22].

This research has progressed due to the development of well-characterized micro- and mesoporous solids with a defined porous structure.

In particular, the large interest in zeolites and their structures derives from their commercial applications that make use of their physical and chemical properties, including pollution abatement, catalysis, cation exchange, and related molecular sieve properties, along with dehydration and rehydration [23].

Zeolites are framework aluminosilicates, occurring as minerals or properly synthesized, whose structure consists of interconnected channels and cavities lodging various cations (mostly Na^+, K^+, Ca^{2+} and Mg^{2+}), loosely bound to the aluminosilicate framework, and water molecules, which can be removed and reabsorbed without structural breakdown [24–26]. Their nominal formula is written as $(M^{q+})_{x/q}Al_xSi_{(y-x)}O_{2y}$, where M^{q+} is the extra-framework cation. The cation balances the formal anionic charge of the framework, due to the presence of aluminium. Aluminium is supposed to be randomly distributed in the framework, except that Löwenstein's rule forbids Al–O–Al bonds [27].

Zeolite chemical formulae, as a rule, do not include OH groups connected to the framework with chemical bonds, but only molecular water. This distinguishes zeolites from other water-containing aluminosilicates, such as clays, micas, vermiculite and obsidian. In particular, this is in contrast to matrices of different nature, the sol–gel glasses, previously used as host systems for H_2O [4].

Even though all zeolite structures are three-dimensional, the bond density in certain crystallographic directions is not always uniform. This non-uniformity of bond density classifies zeolites into (1) those with a lamellar-type structure with aluminosilicate sheets weekly bonded to one other; (2) those with a three-dimensional framework structure with uniform bonding; (3) those with a fibre-like structure with weakly cross-linked aluminosilicate chain units. K-chabazite and scolecite, the samples under investigation, belong to groups number (2) and (3), respectively.

Inside the zeolitic channels, the behaviour of water molecules is the result of a balance between host–guest and guest–guest interactions, i.e. between the interactions, via hydrogen-bond and/or ion–dipole interactions, of H_2O molecules with their water neighbours and with the zeolitic framework and extra-framework cations.

In this context, the knowledge of the interactions between water, the zeolite cations, and the zeolite framework atoms for a wide set of structure may be of paramount interest for synthesis and material science research.

In particular, the use of Fourier transform infrared spectroscopy (FTIR) in attenuated total reflectance (ATR) geometry represents an excellent opportunity for the study of the hydrogen bonding, allowing one to obtain infrared spectra free from saturation artefacts [28]. In this context, the analysis of the intramolecular O–H stretching and H–O–H bending vibrational

modes is the most reliable method for probing, indirectly, the intermolecular network of water, since these contributions are sensitive to the level of interactions of the molecules with the surroundings [29].

There have been a large number of vibrational spectroscopic studies of the H_2O molecules and hydrogen bonding in different substances [30–37].

Very recently we investigated, by the FTIR-ATR technique, the influence of ion-exchange on vibrational dynamics of water confined in the LTA framework (from here on also referred as A) of Na-A and various Mg-exchanged A-type zeolites, by following the evolution of the O–H stretching band as a function of temperature [38]. We remark that, for these kinds of samples, both host–guest and guest–guest interactions are allowed. As main results, water molecules are proved to be involved, even upon confinement, in extended transient H-bonded networks with a high degree of connectivity, and their population increases by increasing the percentage of induced ion-exchange.

These findings are interpreted as an evidence of a 'structure-maker' role played by the LTA framework on physisorbed water, systematically enhanced by increasing the Mg^{2+} content.

Moreover, the existence of a bifurcated H-bond (BHB) among three water molecules has been revealed in the whole explored T-range. The corresponding population factors are observed to decrease with T in the case of the tetrahedral networks, and to increase as far as distorted (BHB) environments are concerned. An interchange between these two involved species is observed, that tends to move towards higher temperature with increasing the percentage of induced ion-exchange.

Here, such an investigation has been, on the one hand, extended to probe the structural status and dynamics of water molecules water in K-chabazite, whose CHA framework has similar topology, dimension and chemical composition to the framework LTA and allows water–water interactions. The spectra, collected in the O–H stretching region from $T = -10\,^{\circ}C$ to $+80\,^{\circ}C$, will be compared with our previous aforementioned FTIR-ATR results on, in particular, Na-A and Mg50-A zeolites, this last one obtained by the Na-A sample by exchanging, in it, the 50% of Na^+ ions with Mg^{2+} ions.

The analysis of the spectra, performed in terms of different levels of connectivity of water environments, will furnish a quantitative picture of the connectivity pattern of water in K-chabazite and, moreover, will allow us to put into evidence similarity and differences in vibrational properties of water in these two kinds of hydrated zeolites.

In addition, our conclusions will be supported by the comparative analysis of new FTIR-ATR results, collected in the H_2O bending mode regions on K-chabazite, Na-A and Mg50-A zeolites.

Finally, new O–H stretching and H_2O bending FTIR-ATR spectra of water in scolecite, a small-pored fibrous zeolite with the framework topology NAT, are collected always in the -10 to $+80\,^{\circ}C$ temperature range. This sample has been chosen for the minimizing of the guest–guest interactions: the nearest neighbours for each water molecule are the cage cations and the framework oxygens, for which the hydrogen-bonding is weaker; there are no water–water contacts at all. The data indicate a more complex molecular interaction of H_2O with the framework and with the extra-framework cations.

2. Experimental details

The samples under investigation were a synthetic K-chabazite ($K_2Al_2Si_4O_{12}\cdot 27H_2O$) with the framework topology CHA, donated by Tosoh Co., Japan, and a natural scolecite ($CaAl_2Si_3O_{10}\cdot 3H_2O$), having the framework topology NAT, coming from Nasik, Maharashtra, India. These

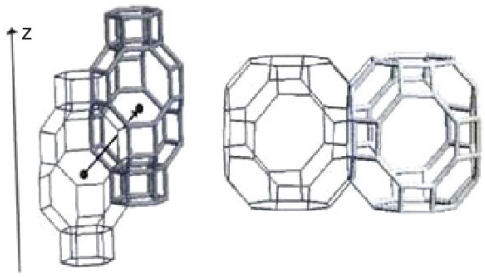

Figure 1. Structure scheme of CHA (left) and LTA (right) frameworks. The vertices mark the positions of Si/Al atoms, and the lines symbolize the oxygen bridges between them.

formulae are given for a unit cell of fully hydrated materials, whose main properties can be found on the International Zeolite Association (IZA-SC) web site [39].

Synthetic Na-A ($Na_{12}Al_{12}Si_{12}O_{48}{\cdot}27H_2O$) and Mg50-A zeolites ($Mg_3Na_6Al_{12}Si_{12}O_{48}{\cdot}33H_2O$), with the framework topology LTA, purchased from Nippon Chemical Industrial Co., Ltd, were also used for a comparative study with the K-chabazite sample. All the samples, in the form of fully hydrated powders, were used without further purification.

Figure 1 illustrates the shape and the interconnectivity of the cages for CHA and LTA frameworks. The structure of chabazite is reported on the left-hand side of figure 1. Each unit cell, which is approximately a hexagonal prism, contains one double six-ring unit (D6R unit) at the top and the bottom [40]. The two fully shaded four-rings connect the top six-ring to the bottom six-ring, while the two half-shaded ones are those which link the D6R units to create the overall lattice. Eight D6R units together enclose an ellipsoidal cavity of ∼6.7 by ∼10 Å. The picture shows two ellipsoidal cages that are connected to each other by eight-rings. The distance between the centres of two such cages is 9.42 Å. In both zeolites the double six-rings can be entered by water molecules. The right-hand side picture shows the cubic structure of LTA zeolites [41]. The large α-cage (cubooctahedral cage) has a free diameter of ∼10 Å and the distance between the centres of adjacent cages is $L = 12.3$ Å. The eight-rings, which are often called windows, have a free diameter of ∼4.1 Å. They build connection between the cages and can be passed by small molecules such as water. The characteristics of interest here that the CHA and the LTA have in common are a spacious cage on one hand and a narrow window between the cages on the other hand.

Scolecite is a calcium zeolite with NAT topology and an ordered (Si, Al) distribution (see figure 2).

It is a fibrous zeolite of the natrolite group. The fibrous morphology is explained by the weakly cross-linked aluminosilicate chains in the framework. In its structure, chains parallel to **c** are composed of four-membered rings of tetrahedra in which opposing tetrahedra are joined by a fifth one [42]. The connection of the chains gives rise to a three-dimensional framework and also defines a well-ordered network of channels.

The location of water molecules in the framework of different types of zeolites and their effect on the location and stability of the zeolites framework and extra-framework cations have been the subject of many experimental and theoretical studies.

The positions of cations and water molecules in hydrated K-exchanged chabazite have been identified by Alberti *et al* [43]. As the main result, the cation site C1 revealed in natural chabazite at the centre of the D6R large cage is shown to be empty in K-exchanged chabazite. Another two cation sites, C2 and C3, have been observed along the ternary axis [111]. Site C2, located near a six-ring of the D6R cage, appears to be occupied by a K^+ ion, whose coordination

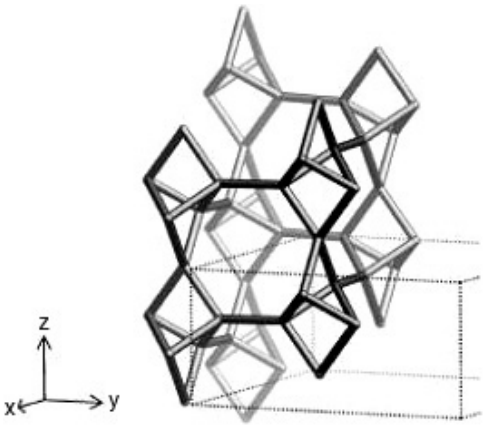

Figure 2. Skeletal NAT framework of scolecite. The vertices mark the positions of Si/Al atoms, and the lines symbolize the oxygen bridges between them.

distances with respect to the framework and the water molecules have been evaluated. Site C3 near the centre of the large cage is also shown to be nearly empty in K-chabazite. The site C4, revealed near the eight-ring window in natural chabazite, is split into two sites close to each other (about 1 Å apart from C4) in the monovalent exchanged form. Water molecules are spread in seven sites, one with 100% occupancy, at the centre of the eight-ring window, the others, normally with low occupancy, inside the large cage.

A detailed description of the location of extra-framework cations and water molecules inside the LTA framework of Na-A and Mg-exchanged A zeolites has already been reported in [38], according to the authoritative results obtained by Gramlich and Meier [44] and Higgins *et al* [45]. As the main result, the preferential locations for Na^+ and Mg^{2+} are calculated to be in the α-cage (in a six-ring window, S6R position) and in the β-cage (in a six-ring window, S6R$'$ position), respectively. This different positioning of bivalent ions leaves free the entrance channels to zeolitic cavities, so causing an 'increase' of the effective section of the pores. Four water molecules are coordinated to the sodium atom. Three of them are in the α-cage, and the fourth one is in the β-cage, perpendicular to the six-ring window where the Na^+ ion is located. Bivalent cations are fourfold coordinated by four water molecules, arranged in tetrahedral configuration.

Finally, as far as scolecite is concerned, the main features of its structure, the location of extra-framework sites by cations and water molecules, have been well known for a long time [46]: chains parallel to **c** are composed of four-membered rings of tetrahedra in which opposing tetrahedra are joined by a fifth one. The connection of the chains gives rise to a three-dimensional framework and also defines a well-ordered network of channels. In the zeolites of the natrolite group, each channel parallel to **c** contains four extra-framework sites. In scolecite, one site is occupied by Ca and the other three are occupied by water molecules.

FTIR studies were carried out on a DA8 Fourier transform infrared (FTIR) spectrometer from BOMEM, using a thermo-electrically cooled deuterated triglycene sulphate (DTGS) detector, in combination with a KBr beamsplitter and a Globar source which is capable of working in the wavenumber range 375–12 500 cm^{-1}. For all the investigated samples, measurements were performed in the T-range -10 to $+80\,^{\circ}C$. The powders were contained in a Golden Gate diamond ATR system, based on the attenuated total reflectance (ATR) technique. As is well known, when infrared radiation, under certain conditions, passes through a prism

made of a high refractive index infrared transmitting material (ATR crystal), it will be totally reflected. When a sample is brought into contact with the totally reflecting surface of the ATR crystal, the evanescent wave will be attenuated in regions of the IR spectrum where the sample absorbs energy. A property of the evanescent wave that makes ATR a powerful technique is that the intensity of the wave decays exponentially with a distance from the surface of the ATR crystal. The distance, of the order of micrometres, makes ATR generally insensitive to sample thickness, allowing for the analysis of thick or strongly absorbing samples. The spectra were recorded in the O–H stretching and H_2O bending mode wavenumber regions, 3000–3800 cm^{-1} and 1500–1800 cm^{-1} respectively. Each spectrum was collected with a resolution of 4 cm^{-1}, and is an average of 100 repetitive scans, so guaranteeing a good signal-to-noise ratio and high reproducibility. No smoothing was done, and spectroscopic manipulation such as baseline adjustment and normalization were performed using the Spectracalc software package GRAMS (Galactic Industries, Salem, NH, USA). Band decomposition was undertaken using the curve fitting routine provided in the PeakFit 4.0 software package, which enabled the type of fitting function to be selected. The strategy adopted was to use well-defined shape components of Voigt functions with all the parameters allowed to vary upon iteration. The statistical parameters were used as a guide to 'best fit'.

3. Results and discussion

3.1. The O–H stretching region

As is well established, an accurate determination of the O–H stretching broad band of water allows the characterization and a quantitative description of the water state by the analysis of the changes in its shape and position.

It is well known that in water the highly isotropic and directional H-bond promotes a variety of intramolecular and intermolecular *transient* (because of the continuous breaking and reforming of the bond) arrangements, with coordination numbers ranging from 0 to 4. From a general point of view, an increasing of the number of hydrogen bonds that a water molecule can establish with its neighbours corresponds to a weaker O–H bond strength of the same molecule, with a consequent shift of the corresponding O–H stretching vibration to the low-frequency region of the spectrum.

So, the spectroscopic investigation of this band allows different substructural components to be recognized, according to populations of water molecules having different mean number of coordination [30, 47].

In our previous FTIR-ATR study of the vibrational dynamics of water in Na-A and Mg-exchanged A zeolites [38] we showed that a satisfying description of the O–H stretching mode can be achieved by resolving the band into components assigned to different types of bulk (internal) and bound (interfacial) water molecules. The curve fitting of the O–H stretching band of K-chabazite has thus been performed by following the same approach used in that paper.

The well-known difficulties [48–50] of uniquely fitting IR band profiles must lead to caution against overinterpretation of the data. The applied procedure, consisting of the evaluation of the minima in the second derivative profile of the measured spectra as a first indication of the peak wavenumbers of the corresponding components of the analysed band, allowed us in some way to overcome this difficulty. Furthermore, we remark that this is a well-established procedure employed in a lot of high-quality published papers when analysing FTIR-ATR O–H stretching spectra of water entrapped in a variety of systems [31, 51], including zeolites [52]. This gives us considerable confidence about the number of bands present and their

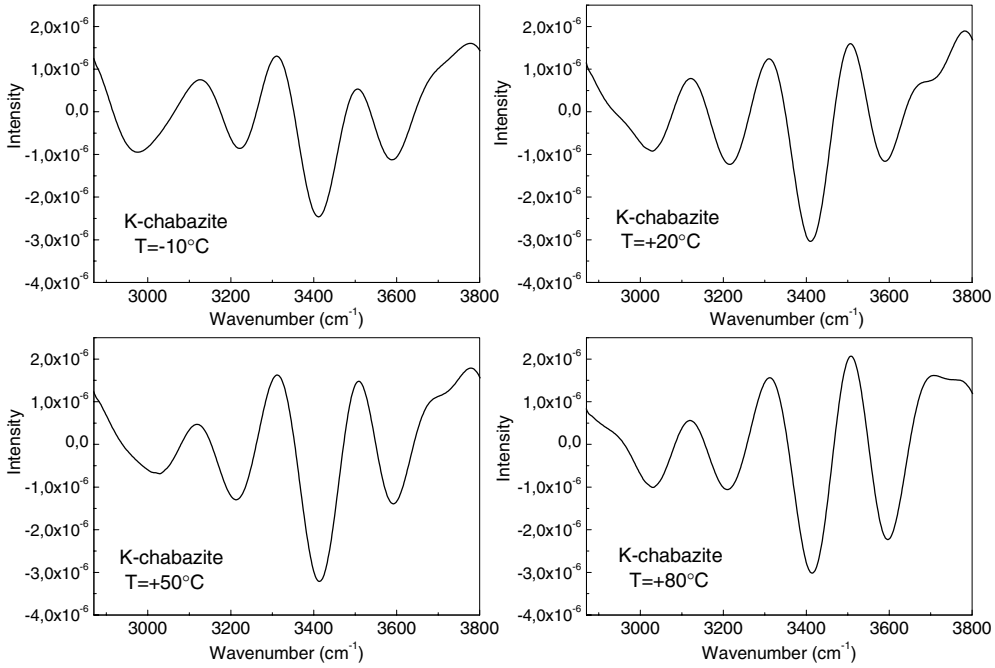

Figure 3. Second derivative diagram of the FTIR-ATR O–H stretching band for K-chabazite at $T = -10, +20, +50, +80\,^{\circ}\mathrm{C}$.

changes in frequency and relative intensity as the water molecule environment changes. Even if it is true that in our case we are looking at water with a high concentration of ions, and hence a description in terms of solvated ionic clusters could be also appropriate, we remark that we are observing intramolecular vibrations, and our description also takes into account the effects on these modes due to cation coordination, as will be seen in the band assignment. In any case, a comparison with molecular mechanics computer calculations could increase, on the one hand, the resolution of standard experiments, and, on the other hand, validate the simulation results.

First of all, we calculated the second derivative of the IR spectra, and the results are displayed in figure 3 at $T = -10, +20, +50, +80\,^{\circ}\mathrm{C}$, as examples.

The diagram of the second derivative clearly evidences four subminima centred at $\omega_1 \sim 3000\ \mathrm{cm}^{-1}$, $\omega_2 \sim 3200\ \mathrm{cm}^{-1}$, $\omega_3 \sim 3400\ \mathrm{cm}^{-1}$, $\omega_4 \sim 3550\ \mathrm{cm}^{-1}$. They indicate the presence, in the spectra, of four sub-bands, peaked at almost the same centre-frequencies, for a very satisfactory description of the O–H spectral profile.

Figure 4 illustrates the corresponding four-component fits for the K-chabazite sample. Notice that the fits of the experimental data are very satisfactory, being characterized by an $r^2 \sim 0.9999$.

In agreement with our previous study [38], the lowest-wavenumber component ω_1 at $\sim$3000 cm^{-1} is ascribed to a new class of water molecules, not present in the bulk phase, for which confinement promotes a hindered vibrational dynamics. They are arranged in a tetrahedral configuration in which four H_2O molecules are coordinated by the extra-framework cation. The sub-band ω_2 at $\sim$3200 cm^{-1} is assumed to arise from large clusters of tetracoordinated water molecules, linked by a linear H-bond, giving rise to a bulk-like structure, in the framework of the model proposed by Walrafen for Raman spectral measurements on liquid water [53]. We remark that the presence, for K-chabazite, of the lowest-energy

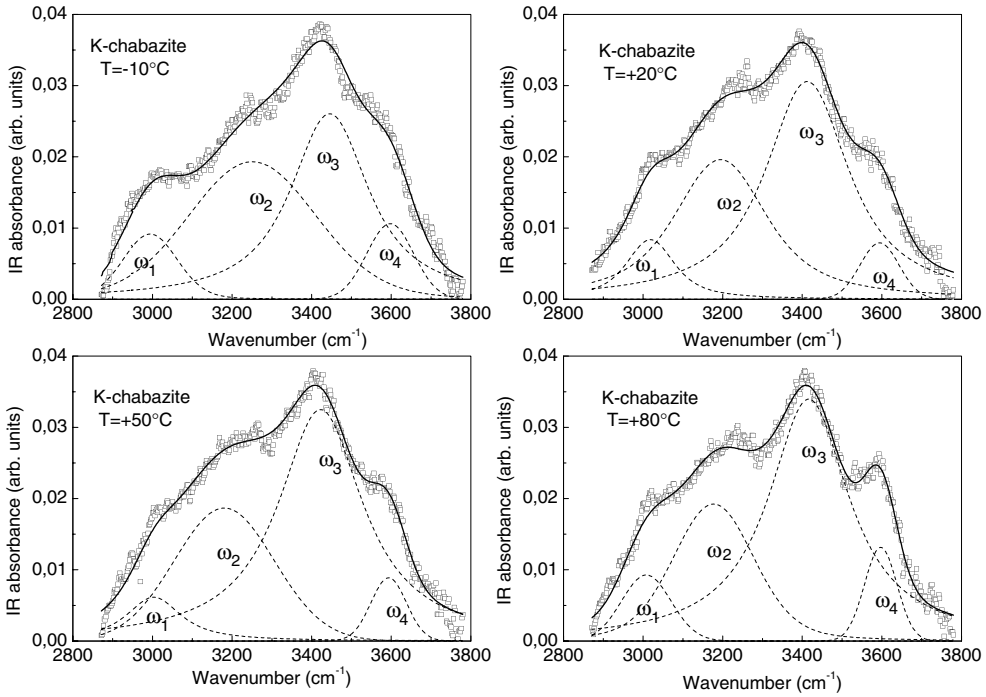

Figure 4. Experimental FTIR-ATR O–H stretching band for K-chabazite at $T = -10, +20, +50, +80\,^{\circ}\mathrm{C}$ (open squares), compared with the fitted curve (solid line) obtained by the decomposition into components (dashed lines).

components ω_1 and ω_2 confirms, also in the case of the CHA framework, the 'structure-maker' role we already assigned, in our previous studies [38, 54], to the LTA framework: in spite of the surface interactions due to confinement and the thermal motion, water molecules can associate in extended stable structures. Component ω_3 at $\sim$3400 cm^{-1} is associated to water molecules not connected in a supramolecular network, but having anyway a degree of connectivity higher than that of dimers and trimers. The origin of this peak suggests, then, the existence of structures with more distorted, bifurcated H-bonds (BHB) [55]. It can express the contribution of those layers of water molecules close to the surface or attached to it, or located at the interface of the aforesaid percolating long-distance networks, or involved in short-lived aggregates. The highest-wavenumber component ω_4 at $\sim$3600 cm^{-1} is attributed to water molecules that behave as dimers exhibiting 'very' weak linear H-bonds, or, more probably, to H_2O interfacial molecules having no contacts with other water molecules. We remark that this picture describes a situation averaged over time, and each molecule is expected to belong to the four types of population over several picoseconds.

Table 1 shows the main fit parameters, i.e. peak wavenumbers and relative areas, of the resolved components for K-chabazite at all the temperatures under investigation.

The peak wavenumbers express the strengths of the respective H-bonds as well as the variations in the average O$\cdots$O distances in the corresponding H-bond network. For each sub-band, the largest observed frequency shift is $\sim$30 cm^{-1}, so we are not able to unequivocally assign a maximum and, hence, we can retain this parameter as constant. The relative areas of the components I_i ($i = 1, 2, 3, 4$) are representative of the variations of the different fractions of H-bonded water molecules assigned to each component.

Table 1. Peak wavenumbers and relative areas of the four spectral components of the O–H stretching band for K-chabazite, Na-A and Mg50-A zeolites in the whole explored T-range.

T (°C)	ω_1 (cm^{-1})	I_1 (%)	ω_2 (cm^{-1})	I_2 (%)	ω_3 (cm^{-1})	I_3 (%)	ω_4 (cm^{-1})	I_4 (%)
K-chabazite								
−10	2996.4	8.3	3211.0	43.7	3413.2	37.7	3597.5	10.3
0	3000.5	8.7	3210.8	38.4	3423.8	42.3	3583.5	10.6
+10	3000.2	8.0	3204.6	35.3	3422.5	48.6	3585.3	8.1
+20	3018.4	7.9	3194.7	34.6	3412.1	53.1	3594.3	4.4
+30	3003.6	7.5	3186.3	31.7	3411.1	56.7	3595.9	4.1
+40	3004.7	6.0	3182.2	27.8	3410.0	59.4	3596.8	6.8
+50	3003.1	5.8	3180.5	27.3	3422.4	61.0	3593.6	5.9
+60	3002.4	5.3	3184.9	25.9	3413.7	65.2	3597.0	3.6
+70	2999.1	5.1	3181.2	24.3	3410.8	66.5	3594.0	4.1
+80	3008.0	4.8	3177.2	23.4	3416.2	66.5	3597.1	5.3
Na-A								
−10	2995.3	8.3	3231.7	50.2	3460.2	37.6	3574.2	3.9
0	3000.0	8.9	3228.3	49.6	3448.2	37.7	3576.0	3.8
+10	2994.7	8.4	3218.0	49.0	3432.7	38.7	3552.4	3.9
+20	2995.2	7.9	3223.1	45.7	3432.8	39.5	3552.4	6.9
+30	2988.4	7.8	3216.5	44.0	3423.0	39.7	3559.8	8.5
+40	2994.2	6.2	3213.9	43.7	3425.7	42.0	3572.3	8.1
+50	3001.5	6.8	3213.4	43.3	3425.6	42.9	3563.6	7.0
+60	3000.8	6.0	3214.1	41.7	3425.5	43.7	3553.9	8.6
+70	2996.4	5.5	3198.9	40.0	3424.1	43.3	3540.6	11.2
+80	2998.5	5.5	3198.7	38.5	3427.8	45.6	3547.2	10.4
Mg50-A								
−10	3006.7	9.5	3167.8	57.6	3378.6	28.6	3517.4	4.3
0	2994.4	9.5	3168.1	55.7	3402.4	29.3	3519.5	5.5
+10	2999.5	9.2	3149.4	52.8	3371.2	31.0	3485.7	7.0
+20	3004.3	9.0	3162.6	50.8	3375.7	33.0	3487.9	7.2
+30	3004.7	8.5	3158.3	50.3	3371.4	33.6	3485.8	7.6
+40	3004.5	8.0	3173.4	50.1	3407.5	33.7	3520.2	8.2
+50	3005.6	7.7	3172.6	48.0	3408.0	34.4	3520.1	9.9
+60	2995.4	7.6	3147.6	46.4	3381.3	37.2	3504.6	8.8
+70	3001.9	7.1	3149.6	43.3	3371.3	39.6	3488.3	10.0
+80	2997.8	6.6	3148.8	42.1	3372.0	41.1	3494.2	10.2

The temperature evolution of the percentage intensities is reported in figure 5. I_1 and I_2 decrease when the temperature is increasing. This is expected, since the thermal motion contributes to destroy long-distance high-connectivity arrangements, favouring less coordinated structures. In fact, an opposite variation is observed for the relative intensity I_3, that definitively makes the BHB the favourite at high T-values. In particular, an interchange between the populations of the dominating species described by I_2 and I_3 has been revealed at $T^* \sim -3\,°C$. Finally, the fact that the relative area I_4 associated to water molecules at the interface remains almost unchanged, can be justified by thinking that their proportion is reasonably not affected by temperature.

Interesting conclusions can be achieved by comparing the spectra of K-chabazite with our previous results obtained in the case of A-type zeolites. In particular, we make reference to

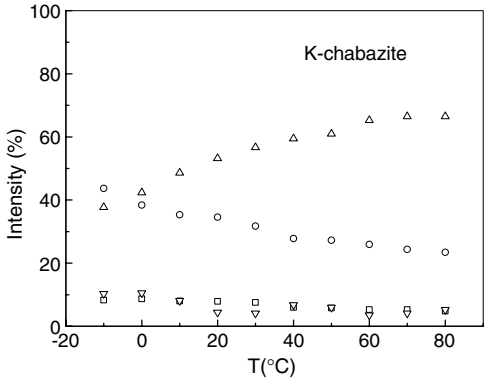

Figure 5. Relative intensities of the decomposition components of the experimental FTIR-ATR O–H stretching band for K-chabazite, plotted as a function of temperature.

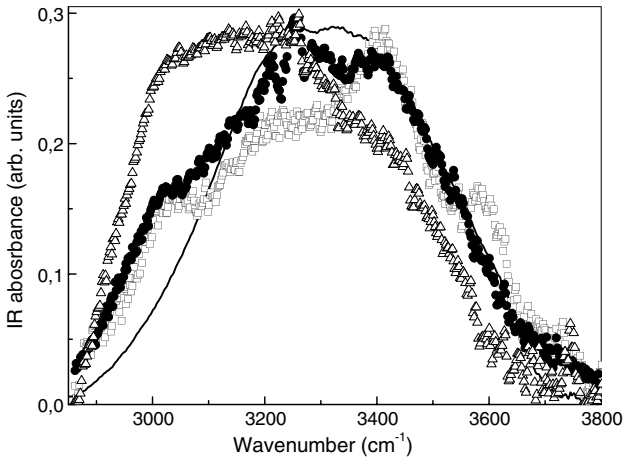

Figure 6. Experimental FTIR-ATR spectra in the O–H stretching region for bulk water (solid line), K-chabazite (open squares), Na-A (closed circles) and Mg50-A (open triangles) zeolites at $T = +30\,^{\circ}\mathrm{C}$.

Na-A and Mg50-A zeolites. Figure 6 shows the O–H stretching experimental IR spectra for K-chabazite, Na-A and Mg50-A zeolites at $T = +30\,^{\circ}\mathrm{C}$, for example, compared with the O–H stretching band of bulk water at the same temperature. As it appears clear, there is a progressive shift of the band maximum towards the low-frequency region. This behaviour recalls what happens in liquid water when the temperature is decreased, and we can hence hypothesize that confinement in zeolites allows water molecules to be involved in arrangements with increasing strength of the H-bonds passing from K-chabazite to Na-A and Mg50-A. This is also confirmed by the decreasing of the wavenumbers of the resolved components, as shown in table 1.

An explanation for this occurrence can be given by taking into account the reduced electronegativity of K^+ with respect to, in order, Na^+ and Mg^{2+}. A reduced electronegativity can favour guest–guest (water–water) interaction in spite of the host–guest (extra-framework cation–water) ones, so allowing the formation of more and more stable arrangements. In addition, the sections of the rings and the channels can be modified by changing the charge and hence the number of cations. The location of cations within the framework will also contribute

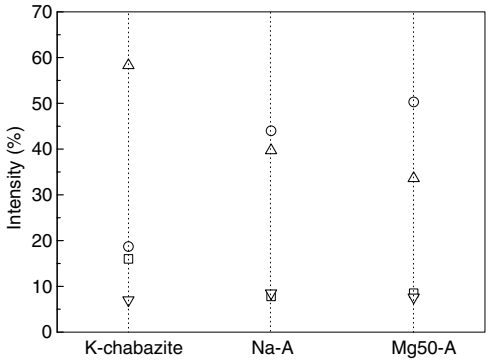

Figure 7. Relative areas of the four O–H stretching sub-bands at $T = +30\,^{\circ}\mathrm{C}$ for K-chabazite, Na-A and Mg50-A zeolites (component ω_1: open squares; component ω_2: open circles; component ω_3: open up triangles; component ω_4: open down triangles).

to the size of pore opening. The theoretical and experimental studies cited in the experimental set-up section [43–46] have widely shown that, for both CHA and LTA frameworks, the presence of monovalent cations gives rise to a smaller effective pore dimension than would be expected for the eight-membered ring framework openings. This is due to potassium (in the case of K-chabazite) and sodium (in the case of Na-A zeolite) ion occupancy of sites where they will partially block the eight-membered ring window. Obviously, since we are considering frameworks with a quite similar topology, the reduction of the pore diameters is enhanced in the case of the larger K^+ ion. In contrast, bivalent cations are proved to preferentially locate in six-ring window adsorption sites at the edges of the supercages, within the voids of the zeolite, and they do not reduce the effective pore diameter. So, the sites inside the supercages are unoccupied and the entrance channels to the zeolitic cavities are left free. Then, we expected, and experimentally verified, that the freer are the cavities, the more favoured will be the formation of stable water clusters.

A broadening of the O–H bands, with respect to bulk water, is also observed, probably linked to an increased variety of rotovibrational states, with a shorter lifetime, explored by the water molecules.

Let us now consider the variations of the relative proportions of the four sub-bands, plotted in figure 7 always at $T = +30\,^{\circ}\mathrm{C}$, as an example.

Actually, for all the analysed samples, the population corresponding to I_1 is small, indicating a tendency, because of confinement, of the 'strongest' fully bonded networks to be broken. Furthermore, in the case of K-chabazite, the bifurcated H-bond (BHB) among three water molecules is shown to be the favourite H-bonding scheme: the corresponding intensity I_3 has the highest value equal to 56.7%, as shown in table 1. On the other hand, the relative proportions $I_1 + I_2$ of the components associated to water molecules with the highest degree of connectivity rapidly increase in passing from the CHA framework of K-chabazite to the LTA framework of Na-A and Mg50-A zeolites, becoming, for these two last samples, the dominant population with an always increasing proportion. This trend can be attributed, on the one hand, to the fact that K^+ ions cause the maximum steric hindrance, since they are the biggest ions considered here, and as explained before they are located at the centre of the cavities. Because of this steric hindrance, the H-bond network rearrangement is difficult. Na-A zeolite occupies an intermediate position: Na^+ ions, even if also located inside the supercages, are smaller than K^+, so reducing this hindrance. Passing from monovalent to bivalent cations, only half

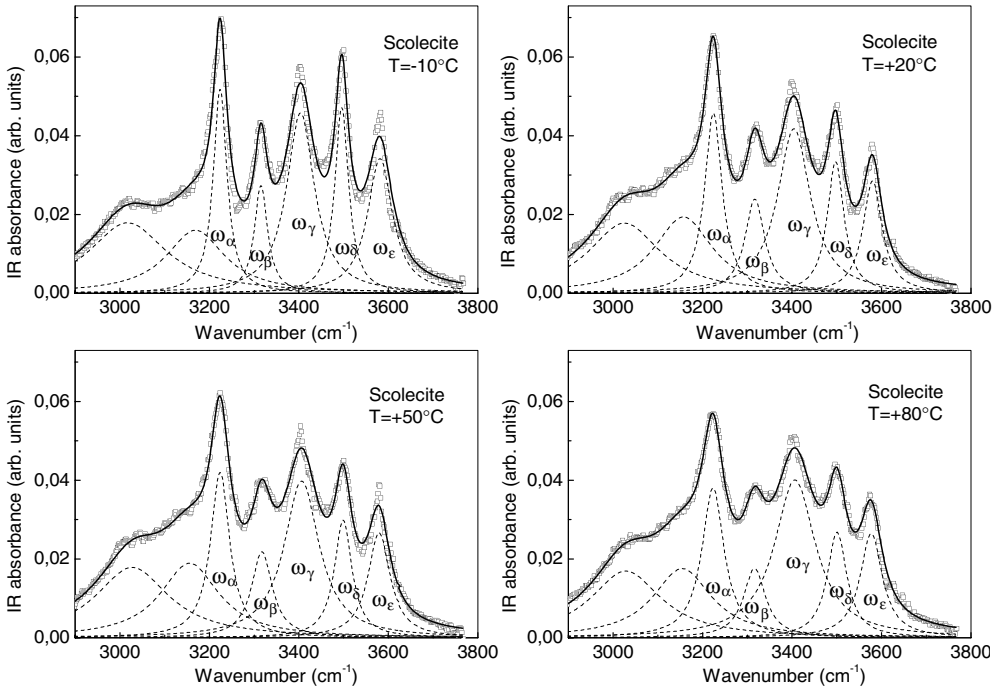

Figure 8. Experimental FTIR-ATR O–H stretching band for scolecite at $T = -10, +20, +50, +80\,^{\circ}\mathrm{C}$ (open squares), compared with the fitted curve (solid line) obtained by the decomposition into components (dashed lines).

the number of cations is needed to compensate the framework charge and, as we said, their different placing increases the section of the zeolitic channels. In this way the steric hindrance is reduced as much as possible, and the number of water molecules that can originate fully developed networks is expected to increase.

All these findings give evidence of a more pronounced 'structure-maker' role of the LTA framework with respect to the CHA one, enhanced by increasing the percentage of the induced ion-exchange. This is also evident from the upshift of the temperature T^* of the interchange indicating the transfer process between the tetrahedral fully bonded networks, whose population decreases with T, and the distorted, not fully developed aggregates, that increase with T. As we said, T^* is $\sim -3\,^{\circ}\mathrm{C}$ for K-chabazite, whereas it turned out to be $\sim +50\,^{\circ}\mathrm{C}$ and $\sim +80\,^{\circ}\mathrm{C}$ for Na-A and Mg50-A zeolites, respectively.

We consider now the case of scolecite that, as already said, is the calcium analogue of natrolite. The interesting point is that, in this case, water molecules are attached only to the framework and extra-framework cations, and not to other water molecules. In figure 8 we report the FTIR-ATR spectra of scolecite collected at $T = -10, +20, +50, +80\,^{\circ}\mathrm{C}$. As can be seen, the spectrum is very complex, since the O–H stretching mode region consists of at least five well-resolved sub-bands, $\omega_\alpha \sim 3224\ \mathrm{cm}^{-1}$, $\omega_\beta \sim 3317\ \mathrm{cm}^{-1}$, $\omega_\gamma \sim 3405\ \mathrm{cm}^{-1}$, $\omega_\delta \sim 3500\ \mathrm{cm}^{-1}$, and $\omega_\varepsilon \sim 3580\ \mathrm{cm}^{-1}$. Two more shoulder peaks at $\sim$3010 cm^{-1} and $\sim$3160 cm^{-1} are also observed in the lower-wavenumber side. These spectral features indicate a more complex hydrogen-bonding between the water molecules and the framework and extra-framework cations. The number of Ca atoms in scolecite is half the number of Na atoms in natrolite, and the number of water molecules per aluminium atom is 1.5 and 1 respectively, for

Table 2. Mean centre-frequencies of the observed sub-bands for scolecite, and corresponding O···O distances. See text for details.

i	ω_i (cm^{-1})	$R_{O\cdots O}$ (Å)
α	3224	2.712
β	3317	2.751
γ	3405	2.802
δ	3500	2.895
ε	3580	3.164

scolecite and natrolite. The additional water molecules give rise to more complex molecular interactions, that originate more complexity in the FTIR-ATR spectra. Two Na^+ and H_2O groups fill the channel space in natrolite, whereas in scolecite the channels are occupied by one Ca^{2+} and three H_2O groups. All six hydrogen atoms of the three water molecules in scolecite form hydrogen bonds to the oxygen atoms of the framework. The water oxygen coordinate the extra-framework cation Ca^{2+}, this last one being also coordinated to four framework oxygen atoms. Stuckenschmidt *et al* [56] evaluated a variety of hydrogen-bond O···O distances between water molecules and the framework ranging between 2.676 to 3.083 Å, with a mean of 2.86 Å. Their relatively small values suggest the presence of a strong hydrogen bond to the lattice, that defines a reorientational order of water molecules. At the same time, the contact O···O distances of the oxygen atoms belonging to Ca-coordinated water molecules turned out to be about 3.3 Å.

The observed sub-bands are linked to the variety of O···O distances defined by Stuckenschmidt *et al* [56], by means of the relation [57]

$$\omega\ (\mathrm{cm}^{-1}) = 3592 - 304 \times 10^9 \left[\mathrm{e}^{(-R_{O\cdots O}/0.1321)}\right] \tag{1}$$

where $R_{O\cdots O}$ represents the O···O distances expressed in angstroms.

By using this relation, we evaluated the $R_{O\cdots O}$ distances corresponding to our observed centre-frequencies. They are reported in table 2. On the basis of the obtained results, we can assign ω_α, ω_β, ω_γ, and ω_δ sub-bands as due to H_2O molecules linked, via hydrogen bonds, to the NAT framework. In contrast, the highest energy sub-band ω_ε can be ascribed to Ca–H_2O coordination.

In the whole explored T-range, the wavenumbers and the percentage intensities of the resolved components appear to be definitely constant. In fact, as far as centre-frequencies are concerned, a maximum shift (with respect to the reported mean values) 3 cm^{-1} wide was revealed, whereas, in the case of the relative intensities, each of them remains constant within, at the most, 6%. This confirms the existence of relatively strong bonds, as already revealed by x-ray diffraction and INS spectroscopy [56, 46].

3.2. H_2O bending region

The effect of confinement was also studied by following the evolution of the water bending mode, around 1650 cm^{-1}.

In bulk liquid water a shift of the maximum towards the high-frequency region is observed when the temperature is lowered. At the same time, the intensity of this band decreases and tends to disappear at crystallization. This last occurrence can be due to the loss of induced transition dipole moment through the bending motion. One can then hypothesize that the H_2O bending vibration can be associated to water molecules not taking part in symmetric tetrahedral networks. Furthermore, the presence of a single absorption band suggests, on the one hand, that this mode does not suffer from the differences in connectivity degree of the surrounding water

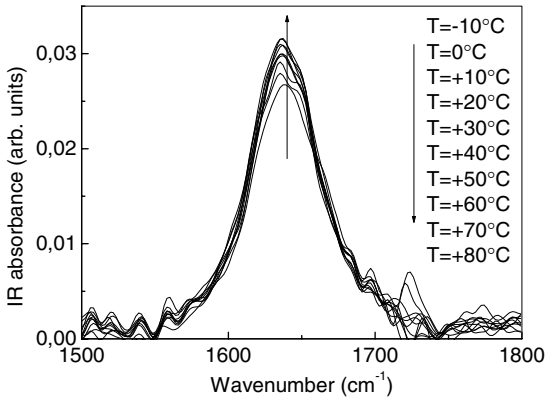

Figure 9. Evolution of the experimental FTIR-ATR H_2O bending spectra for K-chabazite in the investigated T-range.

arrangements, and, on the other hand, makes the analysis of this spectral region easier with respect to the multiple-band highly convoluted O–H stretching zone.

The evolution, as a function of temperature, of the FTIR-ATR H_2O bending spectra for K-chabazite is shown in figure 9.

The revealed trend is the same as that seen in the bulk liquid phase. As the temperature is increased, the H_2O bending band swells over its low-frequency wing, with a corresponding shift of the band maximum towards lower energies, from $\sim$1640 cm^{-1} to $\sim$1635 cm^{-1}. At the same time, the observed intensity increases by $\sim +17\%$. The observed behaviour can be explained by taking into account the enhancement of the thermal motion with increasing T, that will contribute to destroy the H-bonded structures having the highest coordination numbers and to increase the population of water molecules poorly connected to their environment.

For water in K-chabazite, the intensity of the H_2O bending band appears relatively high even at the lowest analysed temperature; its maximum is, in fact, $\sim$0.032 at $T = -10\,^{\circ}$C against $\sim$0.026 at $T = +80\,^{\circ}$C. A similar behaviour is observed for water in Na-A and Mg50-A zeolites (for which the H_2O bending intensity decreases, respectively, by $\sim$23% and by $\sim$18% in the whole explored T-range). In contrast, for water in the bulk state, infrared spectroscopy measurements performed by Brubach *et al* [29] showed an almost flat profile at $T = +9\,^{\circ}$C. We can then hypothesize that, below crystallization, confinement in K-chabazite allows some not fully H-bonded structures, apart from the extended connective tetrahedral networks, to survive. In support of this finding, we remark that it has been largely proved, by means of a variety of techniques, that water in different substrates [58] shows a dynamic behaviour similar to that of bulk supercooled water. In this sense, it would be interesting for the phase diagram of water to investigate the lowest temperature at which water in K-chabazite can be supercooled. For this reason, new FTIR measurements are planned, going down in temperature by the employment of appropriate ATR cells.

In figure 10 the experimental FTIR-ATR spectra of the H_2O bending region for K-chabazite are compared with those obtained in the case of Na-A and Mg50-A zeolites, at $T = 0, +30, +60\,^{\circ}$C as examples.

As displayed in the figure, the intensity of this band decreases on passing from, in order, K-chabazite to Na-A and Mg50-A samples. The lowest bending frequency is found in the K-chabazite sample, while Na-A and Mg50-A zeolites show higher and higher bending frequencies. This trend reveals, in perfect agreement with the results obtained from the analysis

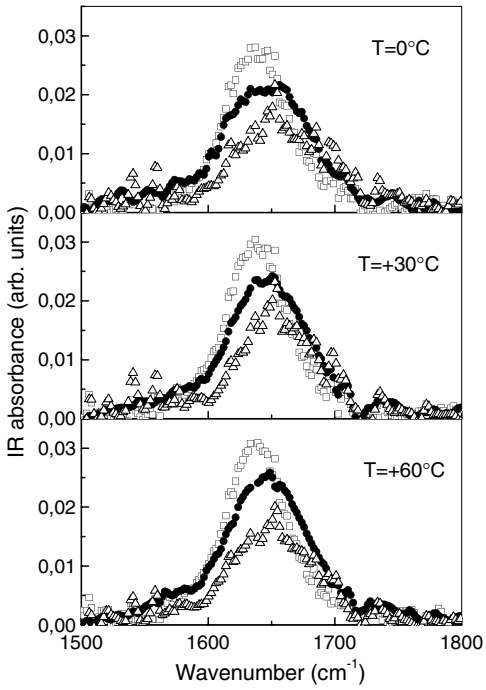

Figure 10. Experimental FTIR-ATR H_2O bending spectra of K-chabazite (open squares), Na-A (closed circles) and Mg50-A (open up triangles) zeolites at $T = 0, +30, +60\,^{\circ}C$.

of the O–H stretching spectral region and widely justified, that the CHA framework allows the smallest fraction of H_2O molecules involved in tetrahedrally coordinated hydrogen bonds with other water molecules and with the framework oxygens. In contrast, the 'structure-maker' role of the LTA framework, in the sense specified above, is confirmed, and, once again, proved to be enhanced by the induced ion-exchange. In this framework, one can think, then, that the force constants associated with the H_2O bending mode of water in K-chabazite are smaller with respect to Na-A and Mg50-A zeolites, and this justifies the positions in wavenumber of the observed bands.

Finally, in the case of scolecite, the existence of a complex H-bonded network is also evident from the experimental FTIR-ATR H_2O bending mode spectrum, reported in figure 11 at $T = -10, +30, +80\,^{\circ}C$ as examples. In a very similar fashion as that found for the O–H stretching mode, water molecules in scolecite have three well-defined bands in the bending region at $\sim$1587, 1647 and 1664 cm^{-1}. In particular, the band at $\sim$1587 cm^{-1} was also observed for thomsonite, another zeolite belonging to the scolecite group [59]. In both cases Ca^{2+} is the extra-framework cation, so we can hypothesize it can reflect the Ca–H_2O coordination and then correspond to the ω_ε sub-band in the O–H stretching region. A first inspection of the figure shows an opposite behaviour of this band with respect to the usual trend observed in the case of bulk water or water confined in CHA and LTA frameworks. Going down in temperature, it shifts towards the low frequencies, from $\sim$1592 cm^{-1} at $T = +80\,^{\circ}C$ to $\sim$1584 cm^{-1} at $T = -10\,^{\circ}C$. An explanation of this behaviour requires a deeper analysis of the H_2O bending vibrational mode, including an assignment of each sub-band and a detailed study of their evolution as a function of temperature. At present this study is in progress and it will be reported in a forthcoming paper.

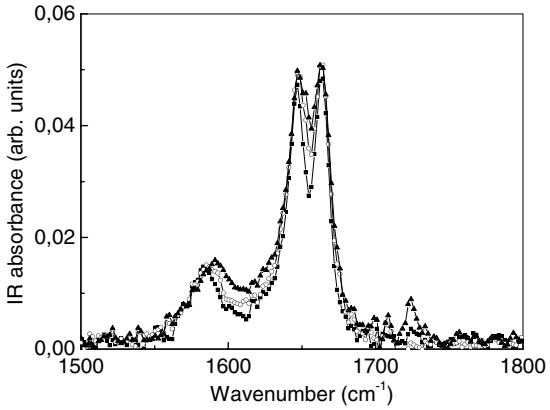

Figure 11. Experimental FTIR-ATR H_2O bending spectra of scolecite at $T = -10\,^{\circ}C$ (closed squares), $T = +30\,^{\circ}C$ (open circles), $T = +80\,^{\circ}C$ (closed triangles). The continuous line is a guide for eye.

4. Conclusions

With the aim to perform an analysis of the vibrational properties of water in different environments, we presented an experimental study, performed in a wide temperature range (-10 to $+80\,^{\circ}C$) by FTIR-ATR spectroscopy, of the O–H stretching and H_2O bending vibrational modes of water in the CHA framework of K-chabazite, in the LTA framework of Na-A and Mg50-A zeolites (in this case the O–H stretching spectra had been previously analysed and the main results are reported just for comparison), and in the NAT framework of scolecite.

The chemical composition and topology of the first two frameworks are similar. For them, the intramolecular O–H stretching band revealed a variety of short-lived H-bonded structures characterized by different mean degrees of connectivity. By means of a four sub-band decomposition of this mode, and by following the temperature-evolution of the main fitting parameters, we have been able to furnish a quantitative picture of collective properties of water according to the nature of the substrate.

In particular, we revealed a new environment of H_2O molecules, not observed for bulk liquid water, whose hindered vibrational dynamics is triggered by the extra-framework cations. We showed that confinement allows water molecules to be involved in a supermolecular bonding scheme with a high degree of connectivity, so revealing, also for the CHA framework, the 'structure-maker' role already hypothesized, in our previous studies, for the LTA framework.

In the case of K-chabazite the perturbation, due to confinement, on the long-distance fully bonded network is the strongest observed, and makes the bifurcated hydrogen bond (BHB) among three water molecules the main feature of the structure of confined water at temperatures above $T^* \sim +3\,^{\circ}C$. This is clearly indicated by the interchange observed in the temperature dependence of the relative population factors.

An explanation to these experimental evidences has been given in terms of electronegativity and size of the extra-framework cations, and taking into account the effect of hydration on the location of cations and water molecules.

The changes in intensity and frequency observed, upon confinement, in the H_2O bending mode, perfectly confirm the results obtained from the O–H stretching analysis. In particular,

for all the analysed samples, evidence of a supercooled behaviour is furnished by going down in temperature to $T = -10\,^{\circ}\mathrm{C}$.

In the case of scolecite, the data collected in the O–H stretching and H_2O bending regions reveal several peaks, probably connected to the existence of three distinct water molecules per Ca^{2+} cation that occupy the channels. The corresponding multiplicity of O···O distances, retained at the basis of the complexity of the FT-IR spectra, has been evaluated. The hydrogen-bond network appears relatively strong, at least in the whole explored T-range. In addition, an unusual temperature-dependence has been revealed for the H_2O bending sub-band related to the Ca–H_2O coordination.

References

[1] Klafter J, Blumem A and Drake J M 1989 *Relaxation and Diffusion in Restricted Geometry* ed J Klafter and J M Drake (New York: Wiley)
[2] Drake J M and Klafter J 1990 *Phys. Today* **43** 46
[3] Alba-Simionesco C, Dosseh G, Dumont E, Frick B, Geil B, Morineau D, Teboul V and Xia Y 2003 *Eur. Phys. J.* E **12** 19
[4] Crupi V, Majolino D, Migliardo P and Venuti V 2000 *J. Phys. Chem.* B **104** 11000
[5] Crupi V, Dianoux A J, Longo F, Majolino D, Migliardo P and Venuti V 2005 *J. Mol. Struct.* **744** 797
[6] Crupi V, Majolino D, Migliardo P and Venuti V 2003 *J. Chem. Phys.* **118** 5971
[7] Rovere M and Gallo P 2003 *Eur. Phys. J.* E **12** 77 and references therein
[8] Bellissent-Funel M C 2003 *Eur. Phys. J.* E **12** 83 and references therein
[9] Webber B and Dore J 2004 *J. Phys.: Condens. Matter* **16** S5449 and references therein
[10] Bruni F, Ricci M A and Soper A K 1998 *J. Chem. Phys.* **109** 1478
[11] Soper A K, Bruni F and Ricci M A 1998 *J. Chem. Phys.* **109** 1486
[12] Crupi V, Majolino D, Migliardo P, Venuti V and Bellissent-Funel M C 2003 *Mol. Phys.* **101** 3323
[13] Bellissent-Funel M C, Chen S H and Zanotti J M 1995 *Phys. Rev.* E **51** 4558
[14] Zanotti J M, Bellissent-Funel M C and Chen S H 1999 *Phys. Rev.* E **59** 3084
[15] Crupi V, Majolino D, Migliardo P, Venuti V and Dianoux A J 2002 *Appl. Phys.* A **74** S555
[16] Crupi V, Magazù S, Majolino D, Maisano G and Migliardo P 1999 *J. Mol. Liq.* **80** 133
[17] Crupi V, Dianoux A J, Majolino D, Migliardo P and Venuti V 2002 *Phys. Chem. Chem. Phys.* **4** 2768
[18] Gallo P and Rovere M 2003 *J. Phys.: Condens. Matter* **15** S145
[19] Gallo P and Rovere M 2003 *J. Phys.: Condens. Matter* **15** 7625
[20] Bergman R and Swenson J 2000 *Nature* **403** 283
[21] Debenedetti P G 1977 *Metastable Liquids: Concepts and Principles* (Princeton, NJ: Princeton University Press)
[22] Teixeira J, Zanotti J M, Bellissent-Funel M C and Chen S H 1997 *Physica* B **370** 234
[23] Bish D L and Carey J W 2001 *Rev. Min. Geochem.* **45** 403
[24] Gottardi G and Galli E 1985 *Natural Zeolites* (Berlin: Springer)
[25] Szostak R M 1989 *Molecular Sieves* (New York: Van Nostrand-Reinhold)
[26] Meier W M and Olson D H 1987 *Atlas of Zeolite Structure Types* (London: Butter-Worths)
[27] Akporiaye D E, Dahl I M, Mostad H B and Wendelbo R 1996 *J. Chem. Phys.* **100** 4148
[28] Maréchal Y and Chamel A 1996 *J. Chem. Phys.* **100** 8551
[29] Brubach J B, Mermet A, Filabozzi A, Gerschel A and Roy P 2005 *J. Chem. Phys.* **122** 184509
[30] Boissière C, Brubach J B, Mermet A, de Marzi G, Bourgaux C, Prouzet E and Roy P 2002 *J. Phys. Chem.* B **106** 1032
[31] Nickolov Z S, Ohno K and Matsuura H 1999 *J. Phys. Chem.* B **103** 7544
[32] Crupi V, Majolino D, Migliardo P, Venuti V and Mizota T 2004 *Mol. Phys.* **102** 1943
[33] Crupi V, Maisano G, Majolino D, Migliardo P and Venuti V 2000 *J. Phys. Chem.* A **104** 3933
[34] Laenen R, Rauscher C and Laubereau A 1998 *J. Phys. Chem.* B **102** 9304
[35] Libnau F O, Christy A A and Kvalheim O M 1995 *Appl. Spectrosc.* **39** 1431
[36] Crupi V, Majolino D, Migliardo P, Venuti V and Wanderlingh U 2003 *Eur. Phys. J.* E **12** S55
[37] Crupi V, Faraone A, Majolino D, Migliardo P, Venuti V and Villari V 2001 *Mol. Phys.* **99** 1525
[38] Crupi V, Longo F, Majolino D and Venuti V 2005 *J. Chem. Phys.* **123** 154702
[39] Database of zeolite structure http://www.iza-structure.org/databases/
[40] Brek D W and Robert E 1974 *Zeolite Molecular Sieves* (Malabar, FL: Kriegar)
[41] Barrer R M 1982 *Zeolites and Clay Minerals as Sorbents and Molecular Sieves* (London: Academic)

[42] Kvik Å, Ståhl K and Smith J W 1985 *Z. Kristallogr.* **171** 141
[43] Alberti A, Galli E, Vezzalini G, Passaglia E and Zanazzi P F 1982 *Zeolites* **2** 303
[44] Gramlich V and Meier W M 1971 *Z. Kristallogr.* **133** 134
[45] Higgins F M, de Leeuw N H and Parker S C 2002 *J. Mater. Chem.* **12** 124
[46] Line C M B and Kearley G J 2000 *J. Chem. Phys.* **112** 9058
[47] Brubach J B, Mermet A, Filabozzi A, Gerschel A, Lairez D and Krafft M P 2001 *J. Phys. Chem.* B **105** 430
[48] Møller K B, Rey R and Hynes J T 2004 *J. Phys. Chem.* A **108** 1275
[49] Rey R, Møller K B and Hynes J T 2002 *J. Phys. Chem.* A **106** 11993
[50] Lawrence C P and Skinner J L 2003 *Chem. Phys. Lett.* **369** 472
[51] Sammon C, Mura C, Yarwood J, Everall N, Swart R and Hodge D 1998 *J. Phys. Chem.* B **102** 3402
[52] Datka J, Boczar M and Gil B 1995 *Colloid Surf.* A **105** 1
[53] Walrafen G E 1974 *Structure of Water and Aqueous Solutions* ed W A P Lucke (Weinheim: Verlag Chemie)
[54] Crupi V, Majolino D, Migliardo P, Venuti V, Wanderlingh U, Mizota T and Telling M 2004 *J. Phys. Chem.* B **108** 4314
[55] Giguere P A 1987 *J. Chem. Phys.* **87** 4835
[56] Stuckenschmidt E, Joswig W, Baur W H and Hofmeister W 1997 *Phys. Chem. Minerals* **24** 403
[57] Libowitzky E 1999 *Monatshefte Chem.* **130** 1047
[58] Bellissent-Funel M C 2001 *J. Phys.: Condens. Matter* **13** 9165 and references therein
[59] Mozgawa W 2001 *J. Mol. Struct.* **596** 129